

Lattice Boltzmann method with selective viscosity filter

Denis Ricot^{a,*}, Simon Marié^{a,b}, Pierre Sagaut^b, Christophe Bailly^{c,d}

^a Renault, Research Advanced Engineering and Materials Department, TCR AVA 1 63, 1 av. du golf, 78288 Guyancourt Cedex, France

^b Institut Jean le Rond d'Alembert, Pierre et Marie Curie University and UMR CNRS 7190, 4 place Jussieu – case 162, 75252 Paris Cedex 5, France

^c Laboratoire de Mécanique des Fluides et d'Acoustique, Ecole Centrale de Lyon and UMR CNRS 5509, 36 av. Guy de Collongue 69131 Ecully Cedex, France

^d Institut Universitaire de France, France

ARTICLE INFO

Article history:

Received 16 July 2008

Received in revised form 19 February 2009

Accepted 15 March 2009

Available online 1 April 2009

Keywords:

Lattice Boltzmann method

Numerical stability

Selective filter

Numerical viscosity

Wavenumber filtering

Bulk viscosity

ABSTRACT

For high-Reynolds number flows, the lattice Boltzmann method suffers from numerical instabilities that can induce local blowup of the computation. The von Neumann stability analysis applied to the LBE-BGK and LBE-MRT models shows that numerical instabilities occur in the high wavenumber range and are due to the interplay between acoustic modes and some other modes. As it is done in the LBE-MRT model, an increase of the bulk viscosity is an efficient way of damping spurious oscillations. However, this stabilization method induces an over-damping of acoustic waves. Some selective spatial filters can be used in order to eliminate the spurious small spatial scales without affecting the large scale physical modes. Three different lattice Boltzmann algorithms based on filtering step are proposed: the fully filtered LBE, the LBE with filtered macroscopic quantities and the LBE with filtered collision operator. The behavior of several explicit filter stencils is studied in the Fourier space. For a given filter stencil, the filtered collision operator approach leads to the highest cut-off wavenumber. In this case, the theoretical wavenumber-dependent viscosity is $\nu(k) = c_s^2 (\tau/[1 - \sigma f(k)] - 1/2)$ where $f(k)$ is the filter shape and σ the filter strength. Under-resolved simulations (high Reynolds number) are performed on the case of the doubly periodic shear layers. The performance of the three filtered LBE is found to be the same as the MRT model for stability control. Propagation of acoustic plane waves is also simulated with the three filtering algorithms. The measured dissipation of acoustic wave compares well with the theoretical results.

© 2009 Elsevier Inc. All rights reserved.

1. Introduction

The lattice Boltzmann method (LBM) is a powerful technique for the computational modeling of a wide variety of complex flow problems [1]. The LBM solves the mesoscopic kinetic equation for particle distributions $g_\alpha(\mathbf{x}, \mathbf{c}_\alpha, t)$, where \mathbf{x} and \mathbf{c}_α are the particle position and velocity vector, respectively, in phase space $(\mathbf{x}, \mathbf{c}_\alpha)$ and time t , and where the macroscopic quantities (velocity and density) are obtained through moment integration of $g_\alpha(\mathbf{x}, \mathbf{c}_\alpha, t)$. The most popular used LBM equation is the single-relaxation-time LBE-BGK model [1]:

$$g_\alpha(\mathbf{x} + \mathbf{c}_\alpha, t + 1) = g_\alpha(\mathbf{x}, t) - \frac{1}{\tau} (g_\alpha(\mathbf{x}, t) - g_\alpha^{\text{eq}}(\mathbf{x}, t)) \quad (1)$$

* Corresponding author. Tel.: +33 1 76 83 20 25; fax: +33 1 76 89 09 29.

E-mail addresses: denis.ricot@renault.com (D. Ricot), marie@imm.jussieu.fr (S. Marié), sagaut@imm.jussieu.fr (P. Sagaut), christophe.bailly@ec-lyon.fr (C. Bailly).

where g_{α}^{eq} is the equilibrium distribution functions. Through Chapman–Enskog multi-scale expansion [1], the non-linear compressible Navier–Stokes equations can be recovered from the simple LBE-BGK equation based on the assumptions that the Mach number is small. The fluid viscosity is related to the relaxation time τ through the relation $\nu = c_s^2(\tau - 1/2)$ where c_s is the sound speed. A well-known stability condition requires that the relaxation time be greater than one-half that corresponds to zero viscosity. The expression of ν suggests that LBM is capable of operating at arbitrarily high-Reynolds number by choosing the relaxation time sufficiently close to $1/2$. However, in this low-viscosity regime, LBM suffers from numerical instabilities that induce unphysical negative values of particle distributions [2]. Moreover, numerical instability waves are often generated by unadapted initial conditions, geometric singularities or in region where large numerical approximations are done (e.g. at the interface of grid refinements). In industrial applications several of these numerical defaults being present, thus computations often become catastrophically unstable. Many solutions have thus been proposed to improve the stability of LBM.

A straightforward idea is to impose a global or local lower bound of the relaxation time τ as it is done in the commercial LBM code PowerFLOW [2,3]. This leads to a lower effective Reynolds number compared to the expected one. This important drawback can be limited by using only a local increase of the relaxation time to insure the positivity of distribution functions [2,4]. But in both approaches, the physical fluid viscosity is modified. An other idea is to add numerical dissipation. For instance, upwind interpolation used in the fractional propagation LB scheme proposed by Qian [5] and Fan et al. [6] introduces numerical viscosity, sometimes called hyper-viscosity. Niu et al. [7] showed that the Interpolation-Supplemented LBM (ISLBM) and the Taylor-Series-Expansion Least-Squares-Based LBM (TLLBM) improve the numerical stability by increasing hyper-viscosities when non-uniform grids are used.

Recent developments of the entropic LBM [8] are attempts to improve stability properties through compliance with a discrete entropy H-theorem. In the same spirit, Brownlee et al. [9] proposed a technique to stabilize the LBM by monitoring the non-equilibrium entropy production defined by $S(g^{eq}) - S(g)$. The main idea is to impose an entropy limiter at points for which the non-equilibrium entropy production exceeds a specified threshold value. Intense and localized corrections [9] can be applied, but smooth functions can be also used to control the additional dissipation [10]. Additional improvements and some theoretical insights are given in [11]. In particular, the most effective choice for the entropy limiter function is shown to be the median entropy filter. It is based on the detection and damping of the strongest non-equilibrium entropy spatial fluctuations. It can be considered as a low-pass filter because it is only active when rapid spatial variation of the non-equilibrium entropy is detected at the nearby neighbors of each grid point. But, unlike selective filter proposed in this paper, this entropy limiter, as well as all the other limiter functions [11] and entropic LBM [8], induces a local modification of the global relaxation parameter. Even if the limiter functions can be very spatially selective, the dissipation is added on all physical wavelengths.

Dellar [12] showed that an enhanced bulk viscosity is useful to improve the numerical stability. In the standard single-relaxation-time model, the bulk and shear viscosities are fixed by the same relaxation time τ . Therefore, Dellar proposed a method that allows the bulk viscosity to be adjusted independently from the shear viscosity by adding a term proportional to the local fluid divergence to the discrete equilibrium distribution. In a more general way the multiple-relaxation-time models [13,14] allow the separation of the relaxations of the various physical and kinetic modes. This separation of relaxation rates is known to be the determining feature of the better stability of LBE-MRT models. In the first part of this paper, we will show that the stability improvement obtained by the LBE-MRT models is associated with an increase of the bulk viscosity that damps out the unphysically-excited acoustic modes. As in Dellar's model, the physical bulk viscosity is artificially increased to get better stability. Even if this stabilization strategy does not modify the effective Reynolds number, it is not suitable for all kind of simulations. For instance, in Computational Aeroacoustics (CAA), propagation of acoustic waves must be calculated accurately. It has been shown that lattice Boltzmann method is an effective scheme to simulate aeroacoustic phenomena [3,15,16] and then a new method is proposed in this work to stabilize LBM simulations without affecting the physical shear and acoustic waves. The idea is based on the use of selective spatial filters that are studied and optimized in the Fourier space. It is worth noting that even if the selective filtering approach is presented in the framework of numerical stability control, the same algorithms can be used in lattice Boltzmann-based Large Eddy Simulations (LES). For instance, selective filters (test filters) are required for the application of dynamic subgrid-scale turbulence models [17]. Large Eddy Simulations that use explicit filtering to replace the dissipative effect of the unresolved subgrid scales are also based on this kind of filters [18].

Presentation of the von Neumann stability analysis of the standard LBE-BGK and LBE-MRT models is reported in Section 2. Several spatial filters are studied in Section 3 and three different filtering strategies are analyzed in the Fourier space. In the last section, the filtering approaches are validated on two benchmark problems.

2. Stability of lattice Boltzmann models with von Neumann analysis

The best way to get insight into stability properties of numerical schemes is to perform a linear stability analysis. The von Neumann method is a classical tool to evaluate the linear stability of numerical schemes and it has been applied in the past to study the standard lattice Boltzmann schemes [19,20], the LBE-MRT scheme [14] and other LBE schemes developed for non-uniform grids [7]. In this section the von Neumann method is quickly presented and is applied on the LBE-BGK and

LBE-MRT model in order to emphasize the causes of the numerical instability growth. In Section 3, this analysis will be also used to investigate filtering effects.

2.1. The von Neumann analysis applied to the LBE-BGK and LBE-MRT models

The von Neumann analysis can be applied to any lattice Boltzmann model but only 2D nine-speed models (D2Q9) are studied for the sake of simplicity. The standard form of the LBE-BGK model is given by Eq. (1) with the equilibrium functions g_x^{eq} :

$$g_x^{eq}(\mathbf{x}, t) = \rho \omega_x \left(1 + \frac{\mathbf{c}_x \cdot \mathbf{u}}{c_s^2} + \frac{(\mathbf{c}_x \cdot \mathbf{u})^2}{2c_s^4} - \frac{|\mathbf{u}|^2}{2c_s^2} \right) \quad (2)$$

where ω_x are weighting factors.

The first step is to linearize the lattice Boltzmann equation (1). The distribution functions g_x are expressed as the sum of a mean part $g_x^{(0)}$ and a small fluctuation part $g'_x(\mathbf{x}, t)$. The mean flow is supposed to be uniform and steady. The non-linear terms of the lattice Boltzmann equation are introduced by products of macroscopic quantities in the equilibrium function (2). This function must be linearized using a Taylor expansion [21]:

$$g_x^{eq}(g_x^{(0)} + g'_x) = g_x^{eq,(0)} + \left. \frac{\partial g_x^{eq}}{\partial g_\beta} \right|_{g_x=g_x^{(0)}} g'_x + o((g'_x)^2) \quad (3)$$

The linearized lattice Boltzmann equation is then obtained by substituting this expression (3) into (1) and removing the mean part.

The von Neumann analysis consists in looking for an harmonic plane wave solution of the linearized equation:

$$g'_x(\mathbf{x}, t) = h_x e^{i(\mathbf{k}\mathbf{x} - \omega t)} \quad (4)$$

With this assumption, the linearized LBE-BGK equation becomes:

$$e^{-i\omega} \mathbf{h} = M \mathbf{h} \quad (5)$$

with $M = M^{\text{BGK}} = A^{-1} \left[I - \frac{1}{\tau} N^{\text{BGK}} \right]$ where I is the identity matrix and A and N^{BGK} are defined by:

$$A_{\alpha\beta} = e^{i\mathbf{k}\mathbf{c}_\alpha} \delta_{\alpha\beta}; \quad N_{\alpha\beta}^{\text{BGK}} = \delta_{\alpha\beta} - G_{\alpha\beta}^{eq}; \quad G_{\alpha\beta}^{eq} = \left. \frac{\partial g_x^{eq}}{\partial g_\beta} \right|_{g_x=g_x^{(0)}} \quad (6)$$

The coefficients of matrix M^{BGK} depend on three parameters which are the relaxation time τ , the wavenumber $\mathbf{k}[k_x, k_y, k_z]$ and the mean flow $\mathbf{U}_0[U_x, U_y, U_z]$. The evaluation and simplification of M^{BGK} can be done with a symbolic mathematical software such as Maple, particularly for the term $G_{\alpha\beta}^{eq}$.

Solutions \mathbf{h} of Eq. (5) are the eigenvectors of the matrix M^{BGK} . Lallemand and Luo [14] use successive approximation of the matrix A in term of k to solve analytically the eigenvalue problem. In the present work, solutions are calculated numerically using linear algebra package LAPACK. The eigenvectors represent the different modes that are supported by the scheme. The transport coefficients of modes are the eigenvalues $\lambda_\alpha = \exp(-i\omega)$. Both eigenvectors and eigenvalues depend on the parameters of the matrix M^{BGK} . In particular, the transport coefficients depend on the wavenumber $\omega(\mathbf{k}) = i \ln(\lambda_\alpha(\mathbf{k}))$. The adimensional wavenumber vector \mathbf{k} represents the number of points per wavelength N_{ppw} :

$$k = \frac{2\pi}{\lambda} \Delta x = \frac{2\pi}{N_{ppw}} \quad (7)$$

In the Chapman–Enskog procedure, the space-time discretization error is neglected. In other words, the Chapman–Enskog procedure supposes that $\Delta t \rightarrow 0$, $\Delta x \rightarrow 0$ which is equivalent to $k \rightarrow 0$ ($N_{ppw} \rightarrow \infty$). On contrary, the von Neumann analysis allows us to take into account space-time discretization errors: these errors make the transport coefficients dependent on the wavenumber [16].

In analogy with the von Neumann analysis of the Navier–Stokes equations [22], the macroscopic transport coefficients are related to the eigenvalues as follows:

$$\begin{cases} \text{Re}[\omega^\pm(\mathbf{k})] = k(\pm c_s(\mathbf{k}) + U_0(\mathbf{k})) \\ \text{Im}[\omega^\pm(\mathbf{k})] = -k^2 \frac{1}{2} \left(\frac{2D-2}{D} \nu(\mathbf{k}) + \eta(\mathbf{k}) \right) \end{cases} \quad (8)$$

$$\begin{cases} \text{Re}[\omega^S(\mathbf{k})] = k U_0(\mathbf{k}) \\ \text{Im}[\omega^S(\mathbf{k})] = -k^2 \nu(\mathbf{k}) \end{cases} \quad (9)$$

where ν is the shear viscosity, η is the bulk viscosity. The superscript \pm denotes the acoustic modes and S is related to the shear mode.

The multiple-relaxation-time model [13,14] has been proposed as an alternative to the standard BGK model. In this model, the collision step is performed in a moment space whereas the propagation step is done in the discrete velocity space. The mapping between the moment space and the discrete velocity space is achieved by a transformation matrix P such that $\mathbf{m} = P\mathbf{g}$. The main advantage of this approach is that a different relaxation time τ_α can be applied for each moment m_α . In particular, the bulk and shear viscosities can be tuned independently. As it will be shown below, the stability improvement obtained with the MRT model results from the increase of the bulk viscosity that damps out numerical waves.

In MRT models, the single-relaxation-time τ of Eq. (1) is replaced by a diagonal matrix S containing the relaxation times:

$$S = \text{diag} \left[\frac{1}{\tau_1}, \dots, \frac{1}{\tau_N} \right] \tag{10}$$

and the general form of the MRT equation is:

$$\mathbf{g}(\mathbf{x} + \mathbf{c}, t + 1) = \mathbf{g}(\mathbf{x}, t) - P^{-1}S[\mathbf{m}(\mathbf{x}, t) - \mathbf{m}^{eq}(\mathbf{x}, t)] \tag{11}$$

In classical MRT [14] the moment equilibrium function \mathbf{m}^{eq} can be deduced from a modified equilibrium function that has been defined in order to reduce the compressible behavior of the LBM [23]. As the acoustic propagation is concerned in this work, the fully compressible equilibrium function given by Eq. (2) is used in our MRT model instead of the incompressible one:

$$\mathbf{m}^{eq} = P\mathbf{g}^{eq}$$

In this case, the linearized MRT collision operator can be expressed directly using the linearized collision operator of the LBE-BGK model N^{BGK} . We have:

$$N^{MRT} = PN^{BGK}P^{-1} \tag{12}$$

With this expression, the matrix M of Eq. (5) becomes:

$$M^{MRT} = A^{-1}[I - P^{-1}SPN^{BGK}] \tag{13}$$

2.2. Stability analysis

The eigenvalue problem Eq. (5) is solved using the LBE-BGK matrix with $1/\tau = 1.99$ and using the LBE-MRT matrix with the relaxation times proposed by Lallemand and Luo [14]:

$$S = \text{diag}[0, 1.64, 1.54, 0, 1.9, 0, 1.9, 1.99, 1.99]$$

The two last relaxation parameters $1/\tau_8$ and $1/\tau_9$ are equal to the relaxation parameter of the LBE-BGK model in order to impose the same shear viscosity. For both models, the mean velocity is set to $U_0 = [0.2, 0, 0]$ and solutions are calculated only for wavenumbers along the x -axis ($k = k_x$). The real and imaginary parts of the angular frequency $\omega(\mathbf{k})$ are plotted as a function of the wavenumber in Figs. 1 and 2. In Fig. 1, we see that the dispersion curves are almost the same for both models. On the contrary, the dissipation curves are very different (Fig. 2(a) and (b)). The nine eigenvalues are plotted on these graphs but only three modes have a physical significance (the two acoustic modes and the shear mode). The other eigenvalues are

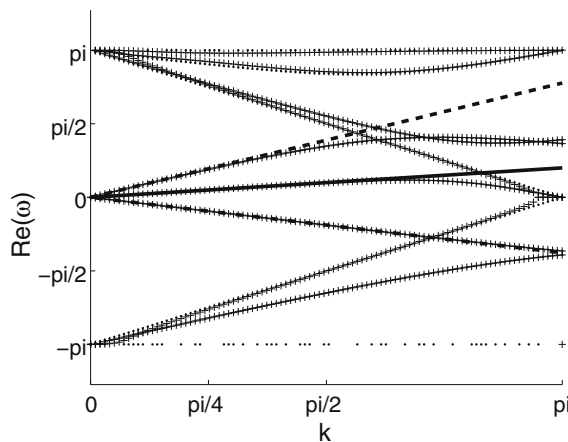


Fig. 1. Dispersion curves of the nine modes of the linearized models with $U_0 = U_x = 0.2$ and $k = k_x$. (.....) LBE-BGK model; (+) LBE-MRT model; (—) expected shear mode dispersion $Re(\omega^2) = kU_0$; (---) expected positive (downstream) acoustic mode $Re(\omega^+) = k(U_0 + c_s)$; (-.-.-) expected negative (upstream) acoustic mode $Re(\omega^-) = k(U_0 - c_s)$.

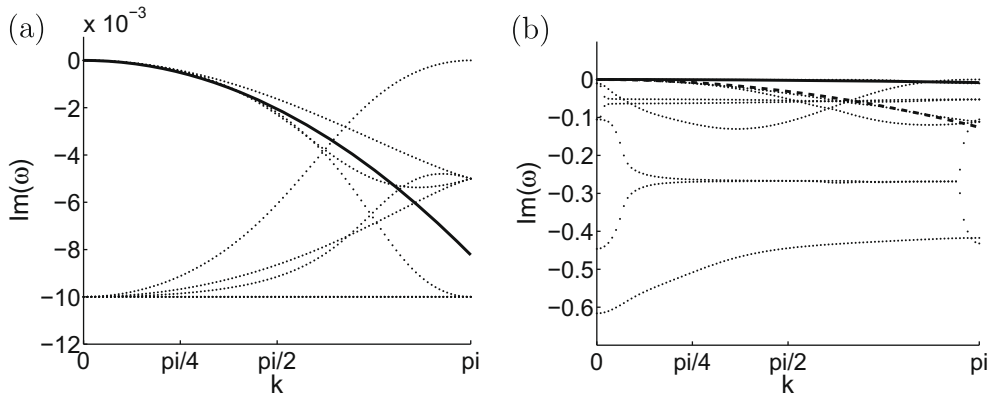


Fig. 2. Dissipation curves of the nine modes of the linearized models with $U_0 = U_x = 0.2$ and $k = k_x$. (a) LBE-BGK model: (.....) calculated dissipation; (—) expected shear mode and acoustic mode dissipation $Im(\omega^s) = Im(\omega^{\pm}) = -k^2 v$. (b) LBE-MRT model: (.....) calculated dissipation (—) expected shear mode dissipation $Im(\omega^s) = -k^2 v$; (---) expected acoustic mode dissipation $Im(\omega^{\pm}) = -k^2((2D - 2)v/D + \eta)/2$.

related to unphysical modes (kinetic modes). Note that points at $Re(\omega) = \pi$ and $Re(\omega) = -\pi$ represent the same kinetic mode. The theoretical transport coefficients predicted by the Chapman–Enskog procedure are also represented. The theoretical propagation speed is U_0 for the shear mode and $\pm c_s + U_0$ for the acoustic modes. The theoretical shear viscosity is $\nu = c_s^2(\tau - 0.5)$ for the LBE-BGK scheme and $\nu = c_s^2(\tau_8 - 0.5)$ for the MRT model. The bulk viscosity of the LBE-BGK scheme is linked to the shear viscosity by the relation $\eta_{BGK} = \frac{2}{D} \nu$. The MRT bulk viscosity is more flexible: $\eta_{MRT} = \frac{2}{D} c_s^2(\tau_2 - 0.5)$.

In the low wavenumber range, the calculated dispersion curves match well the theoretical ones. Above $k \approx \pi/2$ a discrepancy between the theoretical and real dispersion relations appears. It can be shown that this dispersion error is due to the space-time discretization of the discrete velocity Boltzmann equation (see [16] for more details). As we can see in Fig. 2, the space-time discretization scheme also implies an error in term of dissipation. The MRT model uses quite large relaxation times for the kinetic modes and the acoustic modes therefore the dissipation of these modes is much larger than in the LBE-BGK model.

In the previous configuration, all the modes are damped ($Re(\omega) < 0$) therefore the numerical stability is ensured. By varying the angle θ between the wavenumber \mathbf{k} and the x -axis, some positive damping rates can be found for the LBE-BGK model. The unstable regions in the plane (k_x, k_y) are plotted in Fig. 3. The same calculation for the LBE-MRT model shows that the damping rates are always negative. In order to study more precisely the cause of instabilities in the LBE-BGK model, the dispersion and dissipation of the three physical modes are plotted in Fig. 4 for $\theta = \theta_1 = 38^\circ$. For wavenumber above $\pi/2$, the dispersion error of acoustics modes is quite important. At wavenumber $k = k_1$, the angular frequency of the positive acoustic mode becomes equal to that of the shear mode. It is clear in Fig. 4(a) that the sudden increase of one of the damping rate that we can see in Fig. 4(b) is associated with this mode coincidence. In this example, it seems that there is an energy transfer from the acoustic mode to the shear mode. The shear damping rate becomes positive while the acoustic damping rate greatly

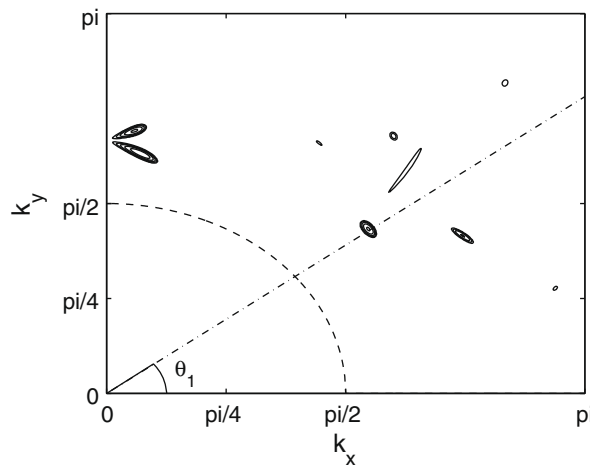


Fig. 3. Linearized LBE-BGK model: maximum positive values of the damping rate $Re(\omega)$ obtained for various wavenumbers with $U_0 = U_x = 0.2$. Isocontours from 0.001 to 0.02 by step of 0.004. The dashed line corresponds to $|\mathbf{k}| = \pi/2$, i.e. four points per wavelength.

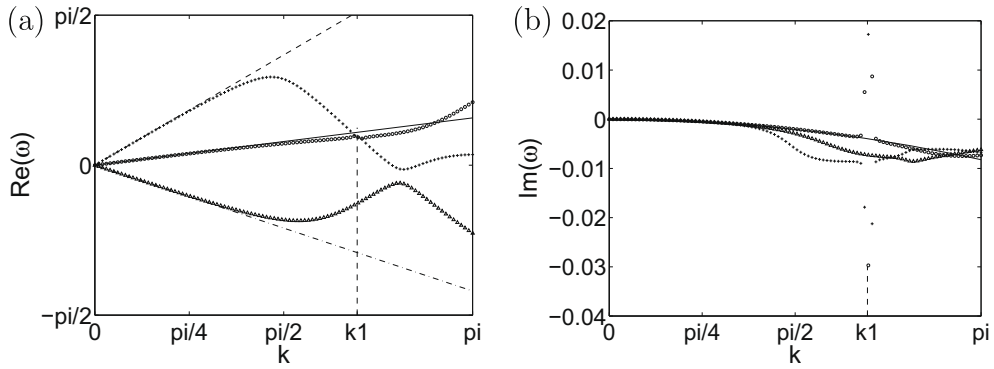


Fig. 4. Linearized LBE-BGK model: (a) dispersion and (b) dissipation of the conserved modes as a function of the wavenumber for $\theta_1 = 38^\circ$. (o) shear mode; (+) positive acoustic mode; (Δ) negative acoustic mode. The theoretical curves are also represented (same representation as in Figs. 1 and 2).

decreases. However, as the modes are merged in the wavenumber range around k_1 , the numerical eigenvalue calculation does not provide a reliable separation of the two modes.

It is quite surprising to observe interplay between modes because the equation system has been linearized around a uniform mean flow. In standard stability analysis of the linearized hydrodynamic equations, mode coupling appears only when there is gradient in the mean flow. It is worth noting that in the linearized lattice Boltzmann equation the mode interplay is not due to a physical coupling between shear and acoustic modes. Instead, mode coalescence is the consequence of space and time discretization errors. Indeed, the von Neumann linear analysis of discrete velocity Boltzmann equation shows [16] that, in absence of discretization errors, mode coalescence never occurs because the theoretical dispersion relations are perfectly recovered.

As for $\theta = 0$ (Fig. 1), the dispersion curves of the LBE-MRT for $\theta = 38^\circ$ are exactly the same as the dispersion curves of the LBE-BGK model. The mode coincidence also occurs at $k = k_1$. The dissipation curves of the LBE-MRT model with the standard relaxation times are shown in Fig. 5(a). The dissipation rates remain negative in spite of the mode coalescence. Now, the value of the second relaxation time τ_2 is set to $\tau_2 = \tau$ in order to have the same bulk viscosity in both LBE-BGK and LBE-MRT models. For this new set of parameters, the dissipation rate exhibits some positive range (Fig. 5b). In particular, we recover the instability region around $k = k_1$. One can also show that the two other positive bumps around $k \approx \pi/2$ are due to the interplay between the two acoustic modes and two kinetic modes. Therefore, we can conclude that the remarkable stability property of the LBE-MRT model is provided by the high value of the bulk viscosity. This approach is very useful for simulating flows for which acoustic phenomena are not taken into account. On contrary, it is not well suited for Computational Aeroacoustics (CAA) applications [24].

3. Selective filtering of the lattice Boltzmann equation

Because the unstable modes we have observed in the previous section have a large wave vector \mathbf{k} (see Fig. 3), some kind of spatial filtering technique may be used as a practical means of reducing the effect of instabilities in LBE simulations. The idea of modifying the hydrodynamic equations by introducing artificial viscosity terms to damp the amplitude of spurious oscillations is discussed in the next section.

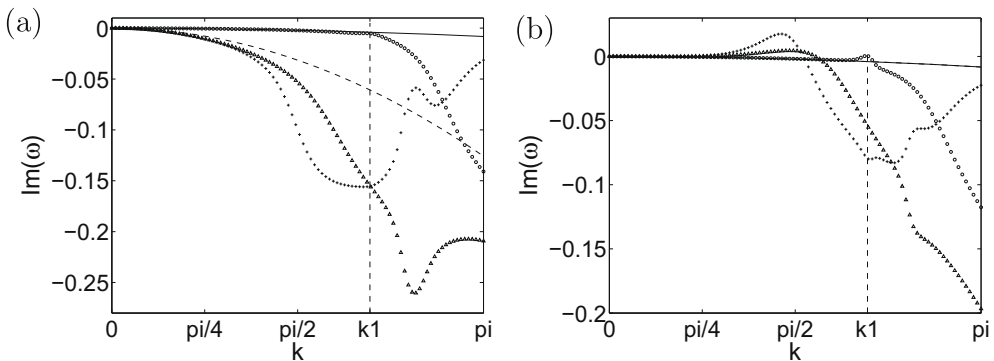


Fig. 5. Linearized LBE-MRT model: (a) dissipation for the standard values of relaxation times and (b) dissipation with $1/\tau_2 = 1.99$ as a function of the wavenumber for $\theta_1 = 38^\circ$. (o) shear mode; (+) positive acoustic mode; (Δ) negative acoustic mode. The theoretical curves are also represented (same representation as in Figs. 1 and 2).

lations near discontinuities was originally proposed by von Neumann and Richtmyer [25] in the context of the Euler equations. This approach is now widely used when low numerical viscosity schemes are to be used. In particular, it is the case in the field of Computational Aeroacoustics [24].

3.1. General presentation of selective filters

The general expression of the filtering operation $\langle \cdot \rangle$ for a given variable v is given by:

$$\langle v(\mathbf{x}) \rangle = v(\mathbf{x}) - \sigma \sum_{j=1}^D \sum_{n=-N}^N d_n v(\mathbf{x} + n\mathbf{x}_j) \quad (14)$$

where N is the number of points of the damping stencil and \mathbf{x}_j are the unit vectors of the D -dimensional Cartesian coordinate system ($D = 2$ in this work). The parameter σ fixes the strength of the filter. It is a constant between 0 and 1, it will be set to 0.1 in the following.

The coefficients d_n are such as $d_n = d_{-n}$ in order to ensure that the filtering operation does not introduce dispersion error [26]. The standard approach [27] for determining d_n consists in cancelling the terms resulting from the Taylor series of Eq. (14) for $k \rightarrow 0$. In this way, the standard selective filters using 5, 7, 9, ... points can be defined. Skordos [28] used a fourth order filter based on the 5-point stencil. In order to achieve a wavenumber cut-off as sharp as possible in the high wavenumber region, Tam et al. [26] optimized the filter coefficients d_n in the Fourier space. This optimization deteriorates the damping behavior, which should be as small as possible, in the low wavenumber range. In the same spirit, Bogey and Bailly [29] developed optimized 9-, 11-, and 13-point damping stencils. The standard 5-point filter used by Skordos referred as SF-5, the standard 7-point filter referred as SF-7, the 7-point stencil of Tam referred as Tam-7 and the 9-point stencil optimized by Bogey and Bailly referred as Bogey-9 will be tested in the following. The filter coefficients are given in Appendix.

In the following part, we will discuss the various possible approaches to introduce the selective filter in the lattice Boltzmann algorithm.

3.2. Fully filtered lattice Boltzmann equation

The first straightforward idea is to filter the distribution functions. The formula

$$\langle g_z(\mathbf{x}, t) \rangle = g_z(\mathbf{x}, t) - \sigma \sum_j \sum_n d_n g_z(\mathbf{x} + n\mathbf{x}_j, t) \quad (15)$$

is applied at each time iteration while the rest of the algorithm remains unchanged. The lattice Boltzmann method with filtered distribution functions can be described as follows:

- (1) Calculate the new distribution function $g_z(\mathbf{x}, t)$ using the standard LBE-BGK scheme (collision, propagation, ...)
- (2) Replace the distribution functions by their filtered values given by Eq. (15)
- (3) Calculate the macroscopic variables with the filtered distribution functions:

$$\begin{cases} \langle \rho(\mathbf{x}, t) \rangle = \sum \langle g_z(\mathbf{x}, t) \rangle \\ \langle \rho u_i(\mathbf{x}, t) \rangle = \sum c_{z,i} \langle g_z(\mathbf{x}, t) \rangle \end{cases} \quad (16)$$

In Eq. (15), the distribution functions $g_z(\mathbf{x}, t)$ are calculated with the standard LBE-BGK scheme applied on the filtered distribution functions of the previous time step:

$$g_z(\mathbf{x}, t) = \langle g_z(\mathbf{x} - \mathbf{c}_z, t - 1) \rangle - \frac{1}{\tau} (\langle g_z(\mathbf{x} - \mathbf{c}_z, t - 1) \rangle - g_z^{(eq)}(\mathbf{x} - \mathbf{c}_z, t - 1)) \quad (17)$$

Substituting this expression of g_z in Eq. (15), we obtain the fully filtered lattice Boltzmann equation. By applying the von Neumann analysis on this new equation, the matrix M of the eigenvalue problem Eq. (5) becomes:

$$M_{(g_z)} = (1 - \sigma f) A^{-1} \left[I - \frac{1}{\tau} N^{\text{BGK}} \right] \quad (18)$$

with the filter function f defined as:

$$f(\mathbf{k}) = \sum_j \sum_n d_n e^{in\mathbf{k}\cdot\mathbf{x}_j} \quad (19)$$

Fig. 6 presents the dispersion and the dissipation of the lattice Boltzmann equation filtered with the standard 7-point stencil. As expected, the dispersion relation is not modified by the filter. In particular, the coupling between the positive acoustic mode and the shear mode still occurs. In the dissipation graph, the sudden increase of the damping rate of all eigenvalues between $k = \pi/4$ and $k = \pi/2$ is clearly visible. Since all the distribution functions are filtered, the damping effect is nearly the same on all modes. The dissipation increase insures that the eigenvalue imaginary parts remain negative in the wave-

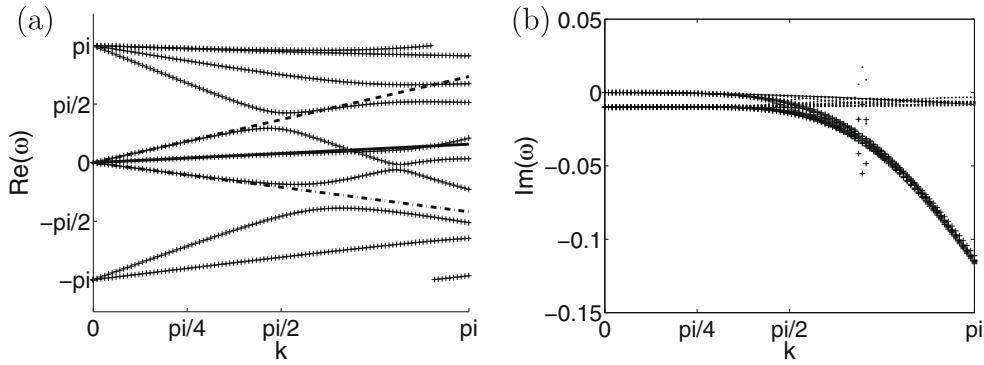


Fig. 6. Linearized LBE-BGK model: (a) dispersion and (b) dissipation of modes as a function of the wavenumber for $1/\tau = 1.99$, $U_0 = U_x = 0.2$ and $\theta_1 = 38^\circ$. (.....) standard model; (+) fully filtered model with SF7. The theoretical curves are also represented (same representation as in Figs. 1 and 2).

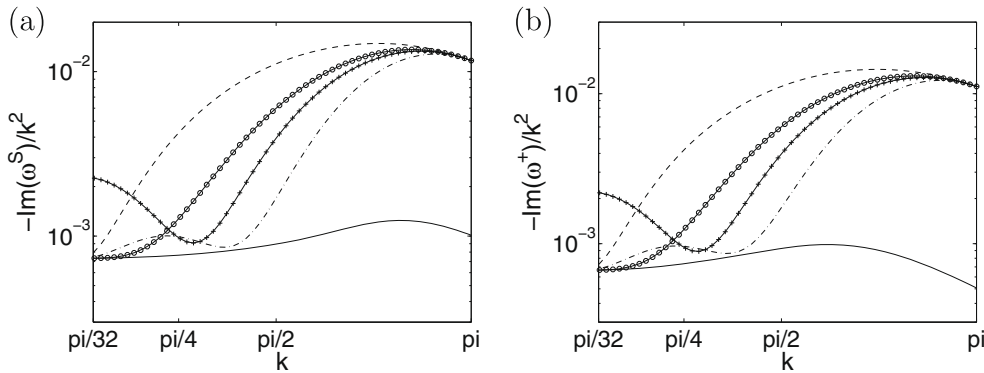


Fig. 7. Effective viscosity of (a) the shear mode and (b) the positive acoustic mode as a function of the wavenumber. (—) without filter; (---) SF-5; (-.-) Tam-7; (-.-.-) SF-7; (-.-.-.-) Bogey-9.

number range where the mode coupling occurs. In order to study more precisely the cut-off wavenumber, the dissipation is plotted in log-scale in Fig. 7. The results obtained with the four filters presented in the previous section are shown. For the sake of simplicity, only the shear mode and the positive acoustic mode are represented. Moreover, the dissipation rate is divided by k^2 in order to obtain the effective viscosity coefficients. Firstly, we see that the bulk and shear viscosities of the standard LBE-BGK model without filter are non-constant. As for the dispersion relation, this wavenumber dependency of the viscous coefficients is due to space-time discretization errors [16]. As already mentioned in Fig. 6(b), the effect of the filters is nearly the same for the shear and acoustic modes. As expected, the cut-off wavenumber of the standard 7-point stencil is higher than that of the 5-point stencil. For a given number of points, the optimization procedure allows to define filters with higher cut-off wavenumber compared to standard filters. Unfortunately, the filter Tam-7 has too high dissipation in the low wavenumber range and should not be used for our applications. The best filter (but also the most expensive in term of computational effort) is the Bogey-9 filter: it is nearly non-dissipative up to $k \approx \pi/2.3 (N_{ppw} \approx 4.6)$. In the rest of the paper, only the standard 7-point filter will be used for theoretical studies and validations.

In this part, the filtering operator has been directly applied to distribution functions. Other filtering strategies can be proposed in the framework of LBM.

3.3. Lattice Boltzmann equation with filtered macroscopic quantities

In the previous part, the fully filtered lattice Boltzmann equation has been established that describes the evolution of the filtered distribution function toward the equilibrium function $g_x^{(eq)}$. This equilibrium function is calculated from the filtered macroscopic variables defined by Eq. (16). It can be written as:

$$g_x^{(eq)} = \langle \rho \rangle \omega_x \left(1 + \frac{\mathbf{c}_x \cdot \tilde{\mathbf{u}}}{c_s^2} + \frac{(\mathbf{c}_x \cdot \tilde{\mathbf{u}})^2}{2c_s^4} - \frac{|\tilde{\mathbf{u}}|^2}{2c_s^2} \right) \tag{20}$$

where the filtered velocity is given by:

$$\tilde{\mathbf{u}} = \frac{\langle \rho \mathbf{u} \rangle}{\langle \rho \rangle}$$

This expression looks like the well-known Favre averaging used in LES theory. In the fully filtered lattice Boltzmann equation both the distribution functions and macroscopic variables are filtered. A new approach can be defined by filtering the macroscopic variables only. Combining Eqs. (16) and (15), the filtered macroscopic variables can be expressed as:

$$\begin{cases} \langle \rho(\mathbf{x}, t) \rangle = \rho(\mathbf{x}, t) - \sigma \sum_j \sum_n d_n \rho(\mathbf{x} + n\mathbf{x}_j, t) \\ \langle \rho u_i(\mathbf{x}, t) \rangle = \rho u_i(\mathbf{x}, t) - \sigma \sum_j \sum_n d_n \rho u_i(\mathbf{x} + n\mathbf{x}_j, t) \end{cases} \quad (21)$$

The main advantage of this new method is that the calculation of the filtered distribution functions is not needed. The gain in term of computational cost is obvious. Following steps now define the new algorithm:

- (1) Calculate the new distribution functions using the standard LBE-BGK scheme Eq. (1)
- (2) Calculate the macroscopic variable from the new distribution functions
- (3) Replace the macroscopic variables by their filtered values Eq. (21)

Using Eqs. (20) and (21), the new linearized matrix can be calculated:

$$M_{g_x^{(eq)}} = A^{-1} \left[I - \frac{1}{\tau} (I - (1 - \sigma f) G^{eq}) \right] \quad (22)$$

The dissipation curves obtained with this new matrix are shown in Fig. 8(a). As for the fully filtered lattice Boltzmann equation, the numerical stability is provided by the dissipation increase in the high wavenumber range. The maximum value of the dissipation rate around $k = k_1$ is slightly higher than the theoretical viscosity dissipation but it remains negative. Of course a greater damping level at this wavenumber can be obtained by using a larger value of strength filter parameter σ . We also remark that the filtering effect is not the same for all modes. This traduces the fact that kinetic and physical modes are not linked to the macroscopic quantities in a straightforward way.

3.4. Lattice Boltzmann equation with filtered collision operator

In the first approach, the full distribution functions are filtered. In the second one, distribution functions are relaxed toward filtered equilibrium quantities but the non-equilibrium parts of distribution functions $g_x^{neq} = g_x - g_x^{eq}$ remain free. Even so, numerical instabilities often occur in high shear flow region [12] where the distribution functions evolve too far from their equilibrium values. Therefore, it seems interesting to apply the selective filter on the non-equilibrium parts of the distribution functions. Since the non-equilibrium functions are dynamically determined by the collision operator, the filtering scheme can be apply on this term of the lattice Boltzmann equation. The third algorithm is:

- (1) Calculate the filtered collision operator $-(g_x^{neq}(\mathbf{x}, t))/\tau$
- (2) Calculate the new distribution functions using the BGK equation with the filtered collision operator:

$$\langle g_x(\mathbf{x} + \mathbf{c}_x, t + 1) \rangle^{coll} = g_x(\mathbf{x}, t) - \frac{1}{\tau} \langle g_x^{neq}(\mathbf{x}, t) \rangle \quad (23)$$

- (3) Calculate the macroscopic variables with the new distribution functions $\langle g_x(\mathbf{x} + \mathbf{c}_x, t + 1) \rangle^{coll}$

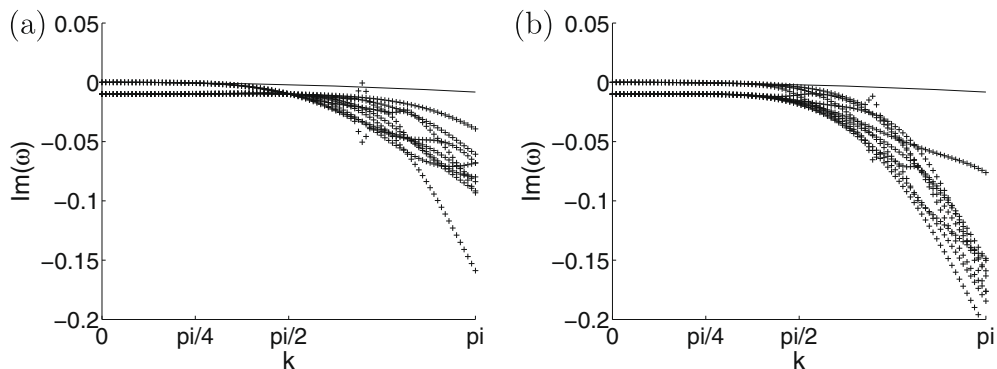


Fig. 8. Dissipation of modes as a function of the wavenumber for $1/\tau = 1.99$, $U_0 = U_x = 0.2$ and $\theta_1 = 38^\circ$. (+) filtered models (filter SF7); (—) theoretical acoustic and shear mode dissipation $-k^2 \nu$. (a) LBE-BGK model with filtered macroscopic variables; (b) LBE-BGK model with filtered collision operator.

For the von Neumann analysis, the matrix of the eigenvalue problem becomes:

$$M_{g_x^{(coll)}} = A^{-1} \left[I - \frac{(1 - \sigma f)}{\tau} N^{BGK} \right] \tag{24}$$

Fig. 8(b) shows the mode dissipation curves induced by this third filtering technique. Again, the eigenvalue imaginary parts remain negative in the whole wavenumber range despite the energy transfer between the positive acoustic mode and the shear mode near the mode coincidence.

We notice that the matrix given in Eq. (24) is the same as that obtained for the standard LBE-BGK model where the relaxation time τ has been replaced by $\tau/(1 - \sigma f)$. Therefore, neglecting the dissipation error related to the space-time discretization, an approximate expression of the effective viscosity can be proposed:

$$\nu(k) = c_s^2 \left(\frac{\tau}{1 - \sigma f(k)} - \frac{1}{2} \right) \tag{25}$$

When applied on the collision operator, the effect of the selective filter can be predicted without von Neumann analysis. The Fourier transform of the filter stencil, which can be easily calculated, is only needed. The validity of the Eq. (25) will be confirmed in the next part (see Fig. 9).

4. Validation on simple flows

We performed numerical experiments to measure the effective viscosity of the two dimensional nine-speed lattice Boltzmann model with the three filtering approaches. We also investigated the effect of the selective viscosity filters on an under-resolved simulation of a Kelvin Helmholtz instability. Both sets of experiments were performed using periodic boundary conditions.

4.1. Dissipation of sound waves

An acoustic plane wave of wavenumber $k = k_x = 2\pi/N$ is initialized in a periodic square domain of size $N \times N$. There is no mean flow ($U_0 = 0$) and the relaxation parameter is set to $1/\tau = 1.99$. The initial perturbation magnitude is sufficiently small to ensure that the propagation stays in the linear regime.

The effective dissipation rate is measured from the decay of the density magnitude. The sinus time signal is wrapped by an exponential dissipation function. The effective viscosity is then calculated by a least squares fit of a straight line to the logarithm of the wrapping function. Simulations have been done for the standard LBE-BGK model and for the three filtered LBE-BGK models. Results are shown in Fig. 9. The theoretical effective bulk viscosity obtained by the von Neumann analysis is also represented for each model. The agreement between the theoretical dissipation curves and the measured ones is very good. In this figure, the expression Eq. (25) is also plotted and the agreement with the measured viscosity for the filtered collision operator model is excellent for low wavenumber. At high wavenumbers, the effective viscosity is not very well predicted by Eq. (25) because this equation does not take into account the space-time discretization error.

It is interesting to note that even if the same filter (SF-7) is used for the three models, the effective viscosity does not exhibit the same spectral behavior. The filtered collision operator model allows to obtain the higher cut-off wavenumber.

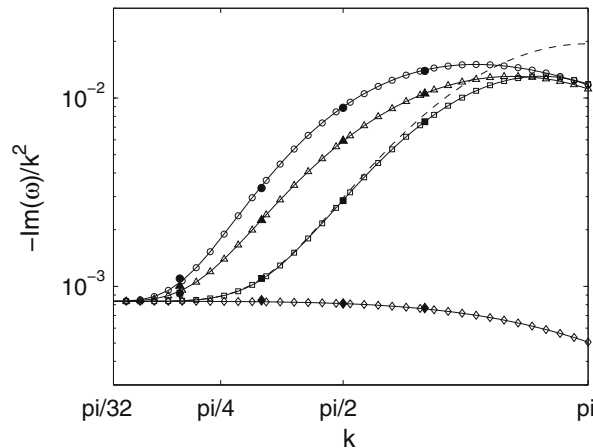


Fig. 9. Comparison of the effective viscosity of the positive acoustic mode for the three filtering approaches. The filter is SF-7 with $\sigma = 0.1$. (\diamond) Without filter; (\circ) fully filtered LBE (\triangle) LBE with filtered macroscopic variables; (\square) LBE with filtered collision operator; (---) Eq. (25). The filled markers are the simulation results.

The most dissipative model is the filtered macroscopic variable model. Of course, for all models, increasing the number of filter points would allow to construct more selective, spectral-like filters.

As shown in Figs. 6(b) and 8 the dissipation of modes subjected to a given filtering approach is nearly the same for all modes. Therefore, it is expected that the efficiency ranking of the three filtering strategies for shear wave dissipation be the same as that observed for sound wave dissipation. This can be checked on a simple shear flow.

4.2. The doubly periodic shear layers

Minion and Brown [30] studied the performance of various numerical schemes in under-resolved simulations of the 2D incompressible Navier–Stokes equations. Dellar [12] also used this simple flow for the validation of its enhanced bulk viscosity LBE model. This simulation is interesting because there is no boundary condition (stability deeply depends on the accuracy and numerical implementation of boundary conditions). Numerical instabilities occur when the shear layers begin to roll-up after some thousand of time step. It is expected that initialization process does not modify the main stability properties of the run. Initial conditions correspond to a perturbed shear layer:

$$\begin{aligned}
 u_x &= \begin{cases} U_0 \tanh(4(y - 1/4)/w), & y \leq 1/2, \\ U_0 \tanh(4(3/4 - y)/w), & y > 1/2, \end{cases} \\
 u_y &= U_0 \delta \sin(2\pi(x + 1/4)), \\
 \rho &= \rho_0
 \end{aligned}
 \tag{26}$$

in the doubly periodic domain $0 \leq x, y \leq 1$. For sufficiently thin shear layer, the parameter w approximates the initial shear layer width. With $w = 0.05$ and a 128×128 grid, there is around 7 points across the shear layer. The parameter $\delta = 0.05$ controls the magnitude of the initial perturbation. The viscosity is $\nu = 0.0001$ and the Mach number is $M = 0.04$. The two shear layers are expected to roll up due to a Kelvin Helmholtz instability excited by the $O(\delta)$ perturbation in u_y . With a 128×128 grid, the shear layer between the Kelvin Helmholtz vortices becomes under-resolved due to stretching as the large vortices roll up. Minion and Brown [30] found that conventional numerical schemes using centered differences became unstable for this under-resolved flow. Even with “robust” or “upwind” Navier–Stokes numerical schemes that suppress

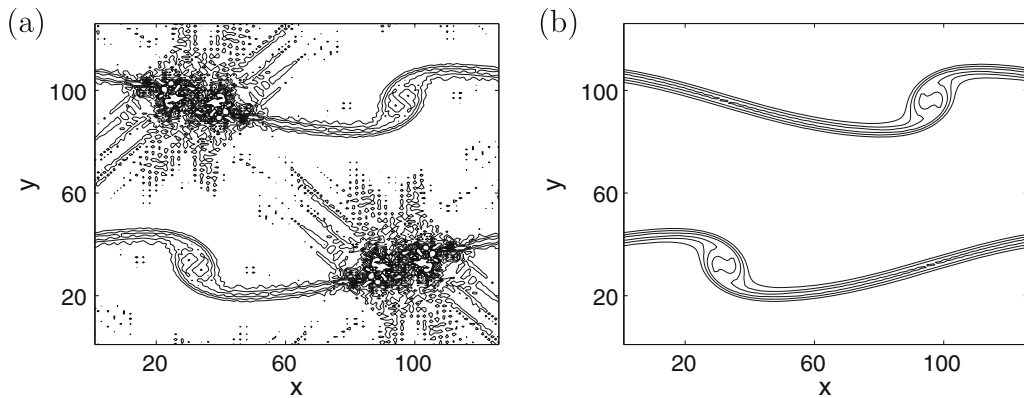


Fig. 10. $|\Omega|$ isocountours from 0.002 to 0.02 by step of 0.003 at timestep $t = 3300$. (a) Standard LBE-BGK model; (b) LBE-MRT model.

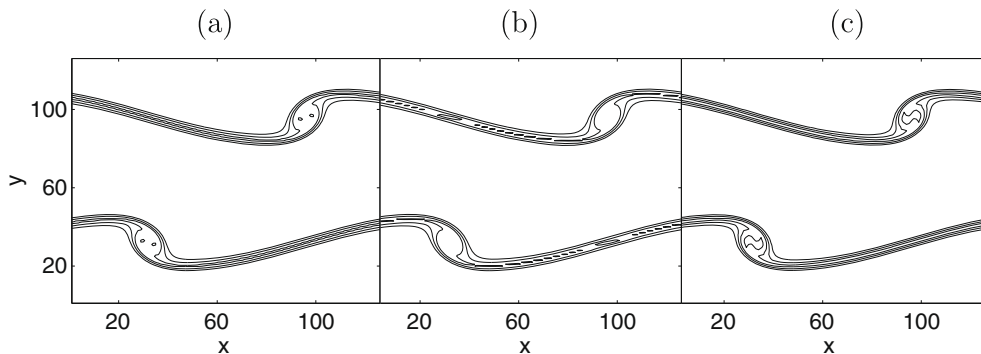


Fig. 11. $|\Omega|$ isocountours from 0.002 to 0.02 by step of 0.003. (a) Fully filtered LBE; (b) LBE with filtered macroscopic variables; (c) LBE with filtered collision operator.

grid-scale oscillations, Minion and Brown showed that two spurious secondary vortices are produced at the thinnest points of the two shear layers. As shown in Fig. 10(a), the same behavior is found with the standard LBE-BGK scheme. The numerical instabilities occur around the secondary shear layer rolling up. As the acoustic waves are not concerned in this simulation, the LBE-MRT model with high bulk viscosity ($1/\tau_2 = 1.64$, $\eta = 0.0366$) can be used to simulate the reference solution (see Fig. 10(b)).

The same flow is then simulated with the three filtered lattice Boltzmann models. For all models, the 7-point stencil is used with $\sigma = 0.01$. The results are displayed in Fig. 11. All filtering approaches lead to stable runs but a careful analysis of the vorticity field in the vortex core shows that the numerical diffusion is not the same for the three models. The less dissipative model is obtained with the filtered collision operator while the most dissipative model is the filtered macroscopic variable model. This result is consistent with the previous conclusions drawn from the simulations of acoustic wave damping.

5. Conclusions

For many applications, the LBE-MRT models and the enhanced bulk viscosity model proposed by Dellar can be well suited for stability control. With these models, the dynamic behavior of flows that are only sensitive to shear viscosity is unchanged. These stabilization models are based on an over-damping of acoustic waves. Indeed, the linear stability analysis shows that numerical instabilities are due to the interplay between the acoustic modes and the shear mode or other kinetic modes. The von Neumann stability analysis also shows that this mode coupling occurs for wavelength smaller than 4 grid-points. This is why the selective filtering approach is particularly adapted for stability control in LBM. The selective viscosity filtering method proposed in this work damps unphysical instabilities without affecting physical shear and acoustic waves. One other advantage of this approach is that the spatial filters can be used as explicit filters in the framework of Large Eddy Simulations.

Three different strategies are proposed to insert some well-known explicit filter stencils into the lattice Boltzmann algorithm. All the three filtering approaches need only few modifications of the standard LBE-BGK scheme. Using a linear analysis in the Fourier space, the dissipative effect of each filtering approach is evaluated as a function of the wavenumber. For a given filter stencil, the higher cut-off wavenumber is obtained with the filtered collision operator model. For this model, the wavenumber-dependent viscosity can be explicitly expressed as a function of the filter shape (Eq. (25)).

All the developments made in this paper are based on the D2Q9 model but the conclusions concerning the stability behavior are also valid for standard 3D models such as the D3Q19 model [31]. High wavenumber instabilities can be also damped using exactly the same filtering algorithms [31]. As the number of distribution function is quite large in 3D, it can be interesting to use the filtered macroscopic quantities approach in order to minimize the computational cost.

In addition to the non-negligible increase of the computational effort, the main drawback of the selective filter schemes is the loss of spatial locality. This drawback is less crippling when block-structured meshes with large grid-blocks are used. Moreover, it is to be noted that some optimized non-centered selective filters and non-uniform grid filters have been proposed [32]. As for the centered schemes, these filters can be easily implemented in the framework of lattice Boltzmann method. They can be useful for physical boundary treatments and for the management of the interfaces between two grid levels in multiple-scale meshes.

In a general way, it is difficult to give the optimal filtering strategy and the best filter stencil and strength coefficient σ because it depends on the simulation parameters (Reynolds number, boundary condition accuracy, ...). For example, simulations of noise generated by flow oscillations over rectangular cavities have been performed [15] using the standard 7-point damping stencil with $\sigma = 0.1$. The filter was applied on the macroscopic variables. The Reynolds number based on the cavity length was 132,000 and the relaxation time was very close to one-half ($\tau = 0.50016$).

Appendix. Selective filters

Coefficients of the explicit selective filters ($d_{-n} = d_n$):

	SF-5	SF-7	Tam-5	Bogey-9
d_0	6/16	5/16	0.287392842460	0.243527493120
d_1	-4/16	-15/64	-0.226146951809	-0.204788880640
d_2	1/16	3/32	0.106303578770	0.120007591680
d_3		-1/64	-0.023853048191	-0.045211119360
d_4				0.008228661760

References

- [1] S. Chen, G.D. Doolen, Lattice Boltzmann Method for fluid flows, *Annu. Rev. Fluid Mech.* 30 (1998) 329–364.
- [2] T. Li, R. Shock, R. Zhang, H. Chen, Numerical study of flow past an impulsively started cylinder by the lattice-Boltzmann method, *J. Fluid Mech.* 519 (2004) 273–300.

- [3] D. Ricot, Simulation numérique d'un écoulement affleurant une cavité par la méthode Boltzmann sur Réseau et application au toit ouvrant de véhicules automobiles, Ph.D. Thesis 2002-36, Ecole Centrale de Lyon, 2002.
- [4] F. Tosi, S. Ubertini, S. Succi, H. Chen, I.V. Karlin, Numerical stability of entropic versus positivity-enforcing lattice Boltzmann schemes, *Mathematics and Computers in Simulation* (Special issue: Discrete simulation of fluid dynamics in complex systems) 72(2–6) (2006) 227–231.
- [5] Y.-H. Qian, Fractional propagation and the elimination of staggered invariants in lattice-BGK models, *Int. J. Modern Phys. C* 8 (4) (1997) 753–761.
- [6] H. Fan, R. Zhang, H. Chen, Extended volumetric scheme for lattice Boltzmann models, *Phys. Rev. E* 73 (2006).
- [7] X.D. Niu, C. Shu, Y.T. Chew, T.G. Wang, Investigation of stability and hydrodynamics of different lattice Boltzmann models, *J. Stat. Phys.* 117 (3–4) (2004) 665–680.
- [8] S. Ansumali, I.V. Karlin, Entropy function approach to the lattice Boltzmann method, *J. Stat. Phys.* 107 (2002) 291–308.
- [9] R.A. Brownlee, A.N. Gorban, J. Levesley, Stabilization of the lattice Boltzmann method using the Ehrenfests' coarse-graining idea, *Phys. Rev. E* 74 (2006) 037703.
- [10] R.A. Brownlee, A.N. Gorban, J. Levesley, Stability and stabilization of the lattice Boltzmann method, *Phys. Rev. E* 75 (2007) 036711.
- [11] R.A. Brownlee, A.N. Gorban, J. Levesley, Nonequilibrium entropy limiters in lattice Boltzmann methods, *Physica A* 387 (2008) 385–406.
- [12] P.J. Dellar, Bulk and shear viscosities in lattice Boltzmann equations, *Phys. Rev. E* 64 (2001) 031203.
- [13] D. d'Humières, Generalized lattice Boltzmann equations, in: B.D. Shizgal, D.P. Weaver (Eds.), *Rarified Gas Dynamics: Theory and Simulations*, Prog. Aeronaut. Astronaut. 159 (1992) 450–458.
- [14] P. Lallemand, L.-S. Luo, Theory of the lattice Boltzmann method: dispersion, dissipation, isotropy, Galilean invariance and stability, *Phys. Rev. E* 61 (2000) 6546–6562.
- [15] D. Ricot, V. Maillard, C. Bailly, Numerical simulation of unsteady cavity flow using lattice Boltzmann method, in: *Eighth AIAA/CEAS Aeroacoustics Conference*, Breckenridge, AIAA Paper 02-2532, 2002.
- [16] S. Marié, D. Ricot, P. Sagaut, Comparison between lattice Boltzmann method and Navier–Stokes high-order schemes for computational aeroacoustics, *J. Comput. Phys.* 228 (2009) 1056–1070.
- [17] P. Sagaut, *Large-Eddy Simulation for Incompressible Flows – An Introduction*, third ed., Scientific Computation Series, Springer-Verlag, 2005.
- [18] C. Bogey, C. Bailly, Computation of a high Reynolds number jet and its radiated noise using large eddy simulation based on explicit filtering, *Comput. Fluids* 35 (2006) 1344–1358.
- [19] J.D. Sterling, S. Chen, Stability analysis of lattice Boltzmann methods, *J. Comput. Phys.* 123 (1996) 196–206.
- [20] R.A. Worthing, J. Mozer, G. Seeley, Stability of lattice Boltzmann methods in hydrodynamic regimes, *Phys. Rev. E* 56 (1997) 2243–2253.
- [21] L.-S. Luo, Lattice-gas automata and lattice Boltzmann equations for two-dimensional hydrodynamics, Ph.D. Thesis, Georgia Institute of Technology, 1993.
- [22] L.D. Landau, E.M. Lifshitz, *Fluid Mechanics*, second ed., Pergamon, Oxford, 1987.
- [23] X. He, L.-S. Luo, Lattice Boltzmann Model for the incompressible Navier–Stokes equation, *J. Stat. Phys.* 88 (1997) 927–944.
- [24] C.K.W. Tam, Computational Aeroacoustics: issues and methods, *AIAA J.* 33 (10) (1995) 1788–1796.
- [25] J. von Neumann, R.D. Richtmyer, A method for the numerical calculation of hydrodynamic shocks, *J. Appl. Phys.* 21 (1950) 232–237.
- [26] C.K.W. Tam, J.C. Webb, Z. Dong, A study of the short wave components in computational acoustics, *J. Comput. Acoust.* 1 (1) (1993) 1–30.
- [27] O.V. Vasilyev, T.S. Lund, P. Moin, A general class of commutative filters for LES in complex geometry, *J. Comput. Phys.* 146 (1998) 82–104.
- [28] P.A. Skordos, Initial and boundary conditions for the lattice Boltzmann method, *Phys. Rev. E* 48 (1993) 4823–4842.
- [29] C. Bogey, C. Bailly, A family of low dispersive and low dissipative explicit schemes for flow and noise computations, *J. Comput. Phys.* 194 (2004) 194–214.
- [30] M.L. Minion, D.L. Brown, Performance of under-resolved two-dimensional incompressible flow simulations II, *J. Comput. Phys.* 138 (1997) 734–765.
- [31] S. Marié, Etude de la méthode Boltzmann sur Réseau pour les simulations en aérodynamique, Ph.D. Thesis, Université Pierre et Marie Curie, Paris VI, 2008.
- [32] J. Berland, C. Bogey, O. Marsden, C. Bailly, High-order, low dispersive and low dissipative explicit schemes for multiple-scale and boundary problems, *J. Comput. Phys.* 224 (2007) 637–662.